Scripta Materialia 276 (2026) 117165

Contents lists available at ScienceDirect

Scripta Materialia

journal homepage: www.journals.elsevier.com/scripta-materialia

Reduction of lateral constrain leads to plasticity in metallic glasses

Rui Yamada [a,*], Keisuke Tabaru [b], Ryota Maeda [b], Wook Ha Ryu [c], Junji Saida [d]

[a] Institute for Materials Research (IMR), Tohoku University, Sendai 980-8577, Japan
[b] Graduate School of Engineering, Tohoku University, Sendai 980-8579, Japan
[c] Department of Materials Science and Engineering, Kumoh National Institute of Technology, Gumi, Gyeongbuk 39177, Republic of Korea
[d] Frontier Research Institute for Interdisciplinary Sciences (FRIS), Tohoku University, Sendai 980-8578, Japan

ARTICLE INFO

Keywords:
Plasticity
Local mechanical state
Inhomogeneous strain/stress distribution
Digital image correlation analysis

ABSTRACT

Inserting a Teflon tape between a relaxed sample of a $Zr_{50}Cu_{40}Al_{10}$ metallic glass and a loading platen resulted in the emergence of a plastic strain of 1.5%–2% under compression. We determined the origin of plasticity from the evolution of the local internal strain/stress state (i.e., the local mechanical state) during compression. A real-time observation of the strain state by a digital image correlation (DIC) analysis revealed a large longitudinal-to-lateral strain ratio ($-\varepsilon_{xx}/\varepsilon_{yy}$) near the contact area, suggesting that the Teflon tape enabled expansion of this region. A finite element method (FEM) analysis confirmed this hypothesis. The DIC analysis revealed the appearance of multiple shear bands, which were initiated in regions that were identified as yielding areas under the expansion contact condition in the FEM analysis. The induced inhomogeneous strain/stress distribution retarded the immediate penetration of shear bands/cracks, which may have led to the emergence of global plasticity.

Metallic glasses are promising for engineering applications because of high strength, a low Young's modulus, a large elastic limit [1,2] and superior workability in the supercooled liquid state [3–6]. However, application is severely limited by catastrophic fracture of these glasses at the final stage of under mechanical stress. There are many reports on plasticity enhancement for metallic glasses by reinforcing a glass matrix with a crystalline phase [7–11], tailoring relaxation state [12–15], heterogeneity [16–20], inducing residual stress [16,21–23], straining during cooling [24]. In these cases, modifying the intrinsic properties of the metallic glass facilitated the formation of multiple shear bands to prevent abrupt fracture.

On the other hand, fracture in metallic glasses during a mechanical test is also strongly affected by extrinsic factors, e.g., the sample size/shape, friction and loading conditions (such as the applied strain rate) [25–29]. Scudino et al. conducted a compression test on a $Zr_{41.2}Ti_{13.8}Cu_{12.5}Ni_{10}Be_{22.5}$ metallic glass in which MoS_2 grease, Teflon tape or Cu foil was inserted between the loading platen and sample as a lubricant to vary the contact condition [26,28]. The stress–strain curve indicated large plastic strains of ~3.5% and ~8% upon insertion of the Teflon tape and Cu foil, respectively. The enhanced plastic deformation was attributed to reduced friction between the sample and loading platen. The inserted Cu foil was considered to facilitate lateral spreading of the material near the sample ends, greatly increasing the plasticity. However, the detailed mechanism for plasticity induction by the lubricant was not elucidated. Because plasticity enhancement was inferred by indirect observation of sample fracture (i.e., after the compression test), it remains to be determined how lubricant insertion affects fracture behaviour (e.g., material flow, evolution of the local strain/stress and initiation, multiplication and propagation of shear bands/cracks upon loading).

Recently, Ryu et al. investigated the fracture behaviour of a $Zr_{65}Cu_{20}Ni_5Al_{10}$ metallic glass and systematically analysed how the plasticity was affected by several extrinsic factors, e.g., the aspect ratio (1.8–4), contact condition (varied by inserting Teflon tape) and Poisson's ratio [29]. A digital image correlation (DIC) analysis showed that Teflon tape insertion produced a relatively uniform shear band distribution throughout the sample. However, the resolution was insufficient to capture the detailed fracture behavior of the sample, e.g., the major shear plane was detected but not the precise crack initiation site. Although serrated flow behaviour was quantitatively analysed, the shear band/crack dynamics (e.g., multiplication and propagation) were insufficiently probed.

In this study, we investigated the origin of plasticity in a relaxed sample of a $Zr_{50}Cu_{40}Al_{10}$ metallic glass under compression using Teflon

* Corresponding author.
E-mail address: rui.yamada.b6@tohoku.ac.jp (R. Yamada).

https://doi.org/10.1016/j.scriptamat.2026.117165
Received 6 October 2025; Received in revised form 16 December 2025; Accepted 4 January 2026
Available online 28 January 2026

tape to vary the contact condition. We observed in-situ fracture behaviour using DIC at a higher spatial resolution than in Ref. [29]. We performed a finite element method (FEM) analysis to determine the evolution of the induced internal stress and its effect on the observed global/local strain. Shear band/crack dynamics were investigated by comparing the DIC and FEM results to elucidate the mechanism of induced plasticity.

A $Zr_{50}Cu_{40}Al_{10}$ metallic glass rod (4 mm in diameter and 8.2 mm long) was prepared by cutting a tilt cast sample. The sample was relaxed by annealing at 740–750 K (T_g+40–50 K) for 2 min followed by cooling at 5 K/min (ULVAC-RIKO, MILA-3000).

Compression tests were conducted (Instron, 5982) using an initial strain rate $\varepsilon_0=5\times10^{-4}$/s, without (Case 1) and with (Case 2) Teflon tape inserted between the loading platen (WC–Co plates) and sample.

A DIC analysis was conducted (LAVISION, DaVis10.2 Strain Master 2DTH) to determine the global and local strains in the sample during the test. In preparation for the analysis, the rod was first ground down to almost half its volume into a semi-cylinder (Fig. 1(a)). A powder was sprayed on the flat sample plane to create a speckle pattern. A camera was used to track the displacement of the speckle pattern to determine the strain at different positions. To generate the stress–strain (σ–ε) curve, the stress was calculated by dividing the applied load by the equivalent-circle diameter and the strain was determined from the global axial strain ($|\varepsilon_{yy}|$) obtained from the DIC analysis. A FEM analysis (ANSYS, Multiphysics 19.2) was conducted (assuming the sample was in the elastic regime) to predict the internal stress state under compression for three contact conditions: i) constrained, ii) free and iii) expansion.

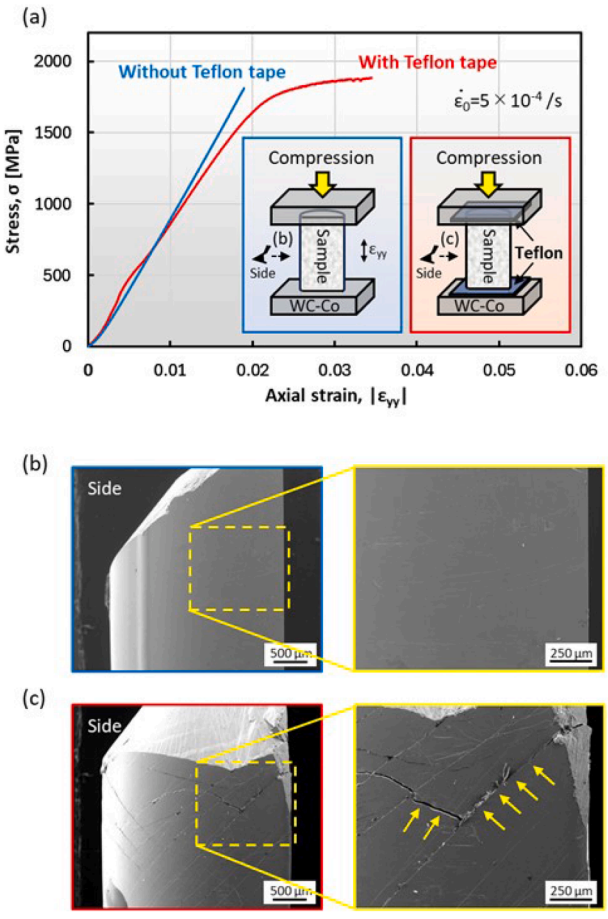

Fig. 1. (a) The stress–strain curve of a relaxed sample of a $Zr_{50}Cu_{40}Al_{10}$ metallic glass with (Case 1) and without (Case 2) Teflon tape inserted between the loading platen and sample. The sample had a semi-cylindrical shape. Side-views of the fractured samples for (b) Case 1 and (c) Case 2.

Each condition was set by changing the Young's modulus and Poisson's ratio of the loading platen and sample, whose values are summarized in Table 1. Contact conditions were as follows; prohibit in-plane motion but allow vertical motion for upper side, prohibit both vertical and in-plane motion for bottom side.

Fig. 1(a) shows the stress–strain curves of the relaxed sample for Cases 1 and 2. At the final compression stage for Case 1, catastrophic fracture at σ_f=1814 MPa (ε_f=0.019) indicated the absence of plasticity. The stress–strain curve for Case 2 gradually became nonlinear above σ≈1500 MPa (ε≈0.017), and final fracture occurred at σ_f=1883 MPa (ε_f=0.03449). More importantly, a plastic strain of approximately 1.5%–2% appeared in the sample, which is similar to those in Refs. [28,29]. Fig. 1(b) and (c) shows side views of the fractured samples, where no distinct shear band appeared for Case 1 and multiple shear bands clearly appeared for Case 2 (indicated by arrows) inducing plasticity.

Scudino et al. [28] reported that the insertion of a soft metal (Cu) reduces friction and exerts pressure near the ends of a glassy sample, facilitating local lateral spreading of the material. These authors argued that an inserted Teflon tape could not exert a large pressure near the sample ends. Consequently, we performed a compression test with inserted Teflon tape to investigate whether material could laterally flow from the center to the ends of the sample near the contact area. We used the DIC analysis to determine the lateral-to-longitudinal strain ratio ($-\varepsilon_{xx}/\varepsilon_{yy}$). Fig. 2(a) shows $-\varepsilon_{xx}/\varepsilon_{yy}$ for Cases 1 (upper left) and 2 (lower left) before fracture (the global strain $|\varepsilon_{yy}|$ is 0.01783 and 0.01558, respectively). Fig. 2(b) and (c) shows line scans of $-\varepsilon_{xx}/\varepsilon_{yy}$. The ratios near the center of the sample average approximately 0.367 and 0.373 for (i) and (iv), respectively, which are relatively close to the Poisson's ratio of the annealed $Zr_{50}Cu_{40}Al_{10}$ metallic glass ($\nu_{\text{strain gage}}$=0.36) [30]. The ratio near the contact area was lower for Case 1 than Case 2 (e.g., ~0.3 at the center of (ii) and ~0.6 at the center of (iii)). The tape enabled the laterally constrained contact area to expand, strongly affecting flow in this region. Fig. 2(a) (upper and lower right) shows the ratio calculated using FEM for the constrained and expansion contact conditions at a global strain of ε=0.023, respectively. The ratio for the constrained condition is lower near the contact area (below 0.31) than for the whole sample (~0.35). The ratio was higher for the expansion condition (0.370–0.531). Different absolute values but similar trends are obtained for $-\varepsilon_{xx}/\varepsilon_{yy}$ using DIC and FEM, suggesting the contact area was constrained for Case 1 and expanded for Case 2. Our experimental evidence of material flow during compression even with inserted Teflon tape contradicts Scuidino's prediction [28].

Fig. 3 shows that different calculated internal stress states under compression for each contact condition. The yielding area is shown in red (assuming a yield strength of 1900 MPa). For the free condition, yielding occurred and immediately spread throughout the sample (ε=2.1437–2.1547). For the expansion condition, a yielding area appeared at the beginning of the test (ε≈2.1327, not shown) and penetrated the whole sample at the final stage of compression (ε=2.2863).

Fig. 4(a) shows the DIC analysis for Case 1. No shear band/crack appears up to final fracture. Fig. 4(b) shows the fracture surface after the test has no discernible shear band. This sudden fracture without an additional shear band is similar to the FEM result for the free condition (Fig. 3, "Free"). However, the measured $-\varepsilon_{xx}/\varepsilon_{yy}$ (Fig. 2) indicated a

Table 1
Each setting parameter (Young's modulus and Poisson's ratio) of loading platen and sample for describing three contact conditions: i) constrained, ii) free and iii) expansion.

		i) Constrained	ii) Free	iii) Expansion
Loading platen	Young's modulus	550 GPa	90 GPa	5 GPa
	Poisson's ratio	0.22	0.36	0.499
Sample	Young's modulus	90 GPa	90 GPa	90 GPa
	Poisson's ratio	0.36	0.36	0.36

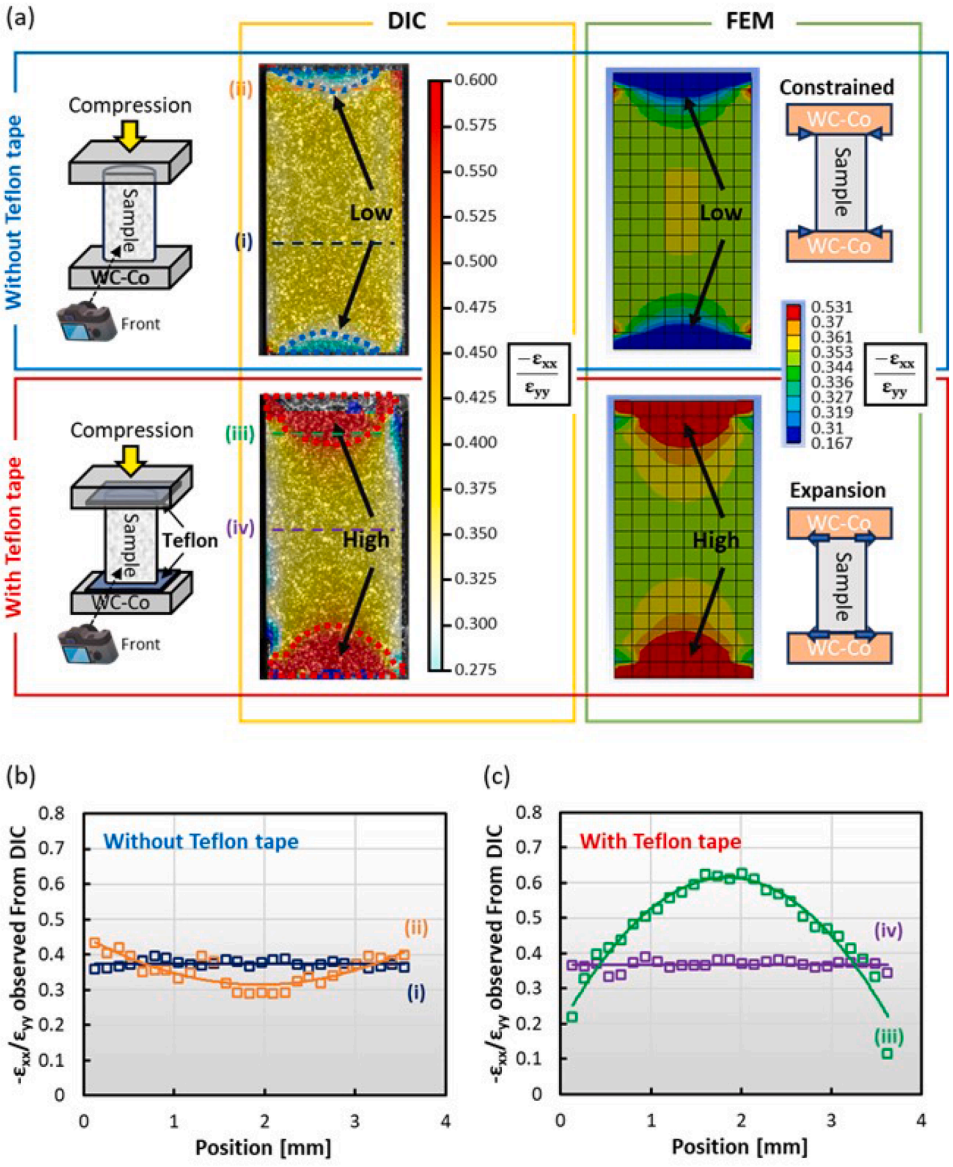

Fig. 2. (a) (Left) The lateral-to-longitudinal strain ratio ($-\varepsilon_{xx}/\varepsilon_{yy}$) of the sample analysed by digital image correlation (DIC) for (upper) Case 1 (no Teflon tape used) and (lower) Case 2 (Teflon tape inserted). (Right) The results of a finite element method (FEM) for $-\varepsilon_{xx}/\varepsilon_{yy}$ assuming constrained (upper) and expansion (lower) conditions for the contact area. Line scan data for $-\varepsilon_{xx}/\varepsilon_{yy}$ for (b) Case 1 and (c) Case 2. The (i)–(iv) curves correspond to the positions marked in (a).

constrained contact area. We explain this discrepancy later.

Fig. 4(c) shows the DIC analysis for Case 2. A shear band/crack first appeared at approximately $|\varepsilon_{yy}|$=0.01641 (Image I), and multiple shear bands appeared with increasing strain (Images II–IV). Fig. 4(d) shows the fractured sample after the test. Multiple shear bands are clearly observed (unlike for Case 1, Fig. 4(b)). Notably, the experimental region with the shear band/crack (Fig. 4(c), Image III) is almost identical to the FEM yielding area for the expansion condition (Fig. 3, "Expansion"). This result supports our hypothesis of an expanded contact area for Case 2 and indicates that a shear band/crack is likely to initiate in a high stress region.

Fig. 4(e) and (f) shows the temporal evolution of the axial strain in the sample (global: ①, ❶; local: (②–③ and ❷–❹). For Case 1, the difference between the global and local axial strains was extremely small (①–③). Enlarging the figure revealed a slightly larger axial strain for ③, indicating a weakly heterogeneous strain/stress distribution. The area ③ appeared very similar to that with the largest stress in the FEM result (Fig. 3, "Constrained" at ε=2.0777). Our analysis of Fig. 4(a) indicated a free contact condition under normal compression, whereas $-\varepsilon_{xx}/\varepsilon_{yy}$ determined by DIC and FEM (Fig. 2(a)) indicated a constrained condition. For Case 2, the large deviation between the curves for ❷–❹ and ❶ indicated a large difference between the global and local axial strains. The curves for ❸ and ❹ lay above the curve for ❶, suggesting perpetually larger local strains than the global strain. The arrow in Fig. 4(f) indicates a large increase in the local axial strain ($|\varepsilon_{yy}|$=0.01855 to 0.0239 for ❸ and $|\varepsilon_{yy}|$=0.01954 to 0.02434 for ❹) compared with the global axial strain ($|\varepsilon_{yy}|$=0.01453), suggesting that the crack was initiated near this point. The axial local strains became similar ($|\varepsilon_{yy}|$=0.0239 for ❸ and 0.02434 for ❹) at a global axial strain of $|\varepsilon_{yy}|$=0.01590 (Fig. 4(f), dotted line I). Thus, the initial crack penetrated ❸ and ❹ simultaneously. The strain in ❹ ($|\varepsilon_{yy}|$=0.04967) considerably exceeded that in ❸ ($|\varepsilon_{yy}|$=0.02686) at a global axial strain $|\varepsilon_{yy}|$=0.01729 (dotted line II). The inset in Fig. 4(f) (an enlargement of Image II in Fig. 4(c)) shows that two different cracks crossed in ❹, where accumulation of the two strains increased the total strain in the area. In ❷, where the cracks did not penetrate until the final fracture, the axial strain first almost tracked the global strain (❶) but its rate of increase decreased approximately after a global axial strain of $|\varepsilon_{yy}|$=0.01729 (dotted line II). The strain in ❷

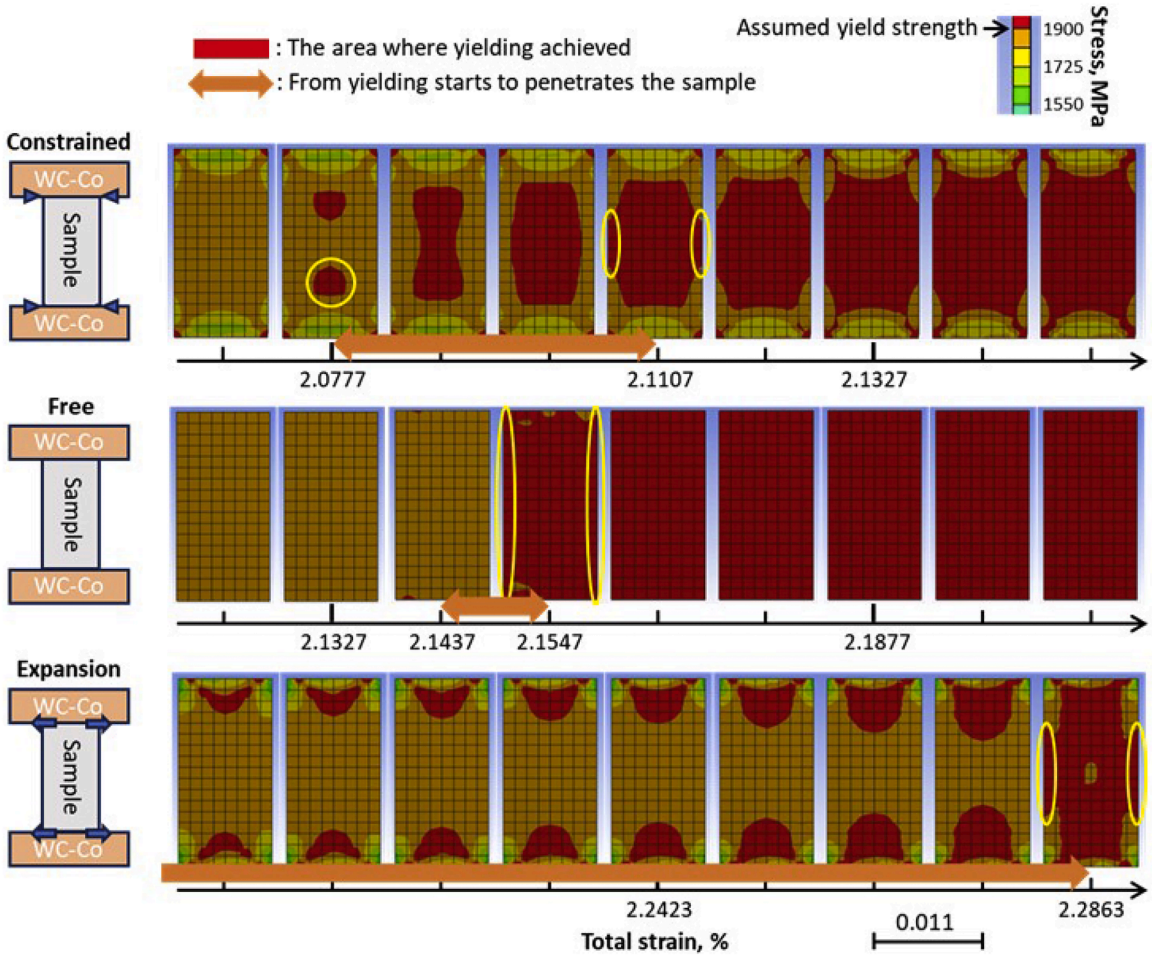

Fig. 3. The calculated evolution of the internal stress state of the sample under compression for different contact conditions: Constrained, Free and Expansion. The horizontal axis shows the total strain under compression, and the colours indicate levels of the equivalent stress in the sample. The area where yielding occurred is shown in red, assuming a sample yield strength of 1900 MPa.

reached at approximately $|\varepsilon_{yy}|\approx0.02$, when global fracture occurred.

Comparing the evolution of the axial strain in each area under different contact conditions shows that a distinct shear band/crack did not appear for Case 1 even at $|\varepsilon_{yy}|=0.01875$ (Fig. 4(a), iii) but had already appeared at $|\varepsilon_{yy}|=0.01590$ for Case 2 (Fig. 4(c), I). This behaviour could be anticipated from the stress–strain curve (Fig. 1(a)), i.e., yielding occurred at a lower strain ($\varepsilon\approx0.017$) for Case 2 than Case 1 ($\varepsilon=0.019$). However, it would be premature to conclude that the shear band/crack initiated at an earlier strain stage for Case 2 because the small scale of the shear bands (e.g. below several tens of micrometers) could not be resolved by DIC. To investigate this issue in detail, serrated flow during compression was analysed for each case. Fig. 4(g) shows an almost constant increment in the stress ($\Delta\sigma=2$–3 MPa) with the axial strain ($\Delta\varepsilon\approx2.6\times10^{-5}$) for Case 1 but increasing deviation in the stress from the average value ($\Delta\sigma\approx2.5$ MPa) with the axial strain for Case 2. This large deviation was ascribed to a serrated flow induced by local shear band/crack formation during compression. The large number of serration events observed for Case 2 were in accordance with the multiple shear bands/cracks observed during the compression test (Image IV in Fig. 4(c)). This deviation did not occur in the stress–strain curve for Case 1 because shear bands/cracks events were almost absent. For Case 2, the deviation began at a considerably lower strain ($|\varepsilon_{yy}|\approx0.01138$) in the experiments (see the arrow in the inset of Fig. 4(g)) than that predicted by DIC ($|\varepsilon_{yy}|\approx0.01453$) (see the arrow in Fig. 4(f)). This result implies that narrow (i.e., premature) shear bands that were difficult to visualize by DIC has already started to appear in the sample for Case 2 at $|\varepsilon_{yy}|\approx0.01138$.

We consequently formulate prediction scenarios for fracture behaviour. Under normal compression (Fig. 5(a)), despite the small observed difference between the local strains (Fig. 4(e), ② and ③), the sample deformed almost uniformly at the early stage ($\varepsilon=0$–ε_1). Further compression resulted in local fracture in the area with the highest strain/stress (shown in orange square, $\varepsilon=\varepsilon_2$). The almost uniform internal strain/stress state enabled the yield strain/stress to be reached in another region almost simultaneously (shown in grey square), leading to immediate global fracture ($\varepsilon=\varepsilon_2$'). The very short strain interval between the first appearance of local fracture and global fracture ($\Delta\varepsilon=\varepsilon_2$'–$\varepsilon_2$) led to unstable shear band/crack propagation, resulting in a nearly single shear band and brittle fracture. For Case 2 (Fig. 5(b)), material flow from the center to the ends of the sample in the contact region induced a heterogeneous stress field and a variable local strain throughout the sample. A shear band/crack first appeared in the area with the highest local strain/stress ($\varepsilon=\varepsilon_1$, shown in light blue square). The yield strain/stress had not been reached in the surrounding material and local fracture had not occurred in most of the rest of the sample (shown in green square), locally constraining the shear band/crack. Under compression, yielding gradually spread to the entire sample, enabling the shear band/crack to propagate until global fracture eventually occurred. The strain interval between the first appearance of local fracture and global fracture ($\Delta\varepsilon=\varepsilon_3$–$\varepsilon_1$) was longer than under normal compression ($\Delta\varepsilon=\varepsilon_2$'–$\varepsilon_2$). For Case 2, local fracture occurred at $\varepsilon=\varepsilon_1$ before that in Case 1 (at $\varepsilon=\varepsilon_2$, where $\varepsilon_2>\varepsilon_1$) but final global fracture was

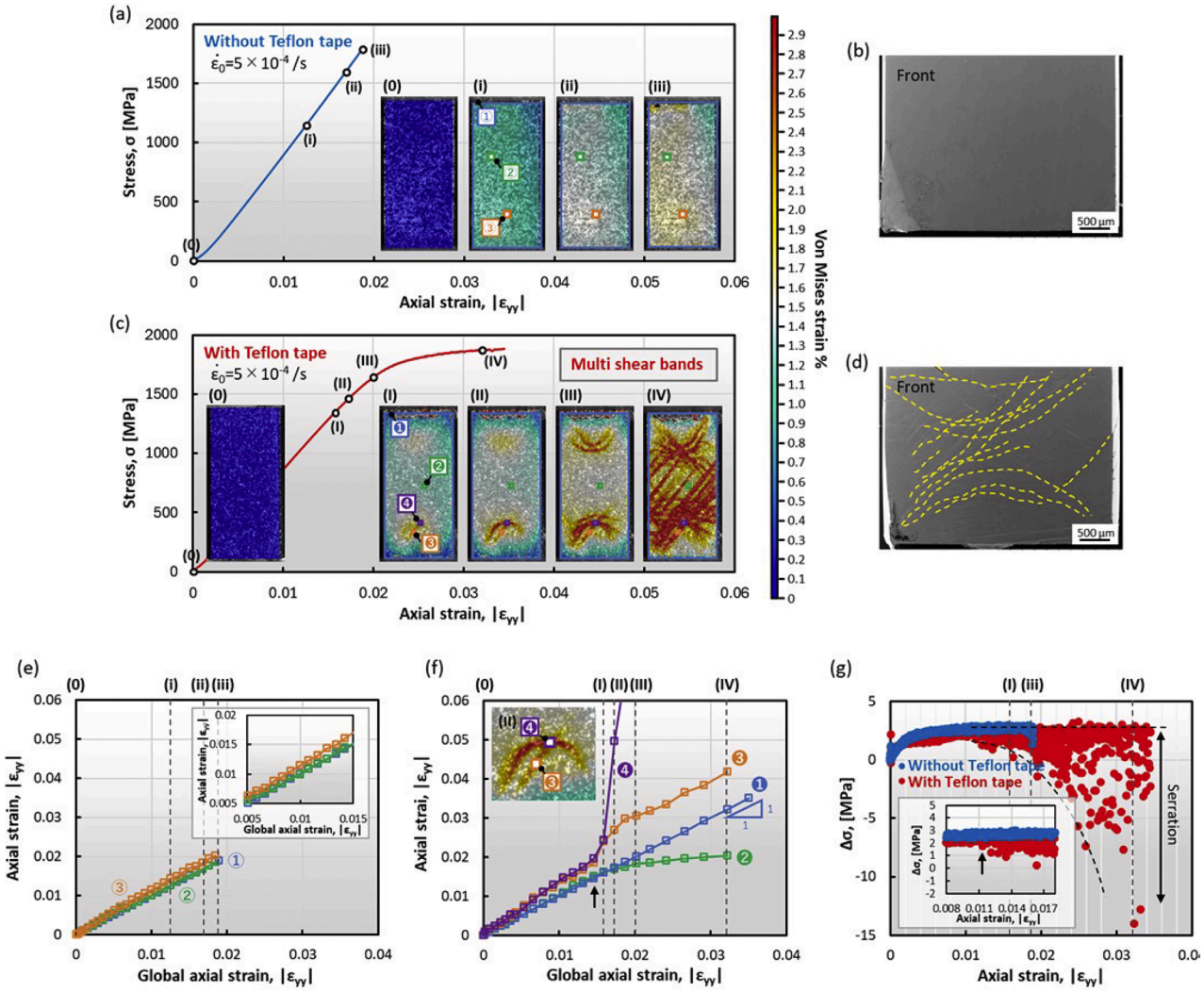

Fig. 4. Case 1 (no Teflon tape used): (a) The results of a digital image correlation (DIC) analysis of the sample during a compression test. (b) Fracture observation of the sample after the compression test. Case 2 (Teflon tape inserted): (c) DIC analysis result of the sample during a compression test. (d) Fracture observation of the sample after the compression test.
Measured axial strain (|ε_{yy}|) versus time for (e) global (①) and local (②–③) areas in Case 1 and (f) global (❶) and local (❷–❹) areas in Case 2. The numbers correspond to the positions shown in (a) and (c). (g) The evolution of the stress increment (Δσ) with the axial strain (Δε≈2.6×10^{-5}) for Cases 1 and 2.

strongly retarded (ε_3>ε_2'). During the interval $\Delta\varepsilon$=ε_3–ε_1, new shear bands/cracks continuously formed throughout the sample and intersected/interfered with each other during propagation, delaying final global fracture. This mechanism could plausibly prevent abrupt fracture and explain the emergence of plasticity for Case 2.

In the present study, we discussed the fracture behavior in a relatively macroscale rather than microscale. Currently, we predicted that the presence of inhomogeneous strain/stress fields under compression creates a distribution of yield region locally within the sample and initiated crack tip is surrounded by the area where yielding has yet occurred, resulting in inhibiting a single shear band propagation. However, we are planning to clarify the underlying mechanism on a tiny scale by addressing the microscale test (e.g. in-situ mechanical test in a SEM) as previously conducted by Glushko et al. [31].

As discussed above, we have demonstrated that the strain/stress state in the sample under compression strongly governed the shear band/crack dynamics. Thus, the strain/stress distribution is an important factor for fracture in metallic glasses, as suggested in several recent reports [25,32–34]. Sohn et al. previously proposed that plastic mechanical behavior (i.e. ductile or brittle) of metallic glasses can be explained by the comparison between $\nabla\sigma_{US}$, the minimum stress gradient over which growth of stable shear band can take place, and the applied stress field $\nabla\sigma_{app}$ [34]. Our present result supports their framework that stress (or strain) gradient is one of the key indicators to determine the plastic properties.

As already mentioned before, previous study revealed that improvement of plasticity occurred when Teflon tape was inserted in a $Zr_{65}Cu_{20}Ni_5Al_{10}$ metallic glass, whose alloy originally shows plasticity even in unlubricated condition [29]. However, to discuss whether it works for a more brittle sample, we investigated a $Zr_{50}Cu_{40}Al_{10}$ metallic glass as-cast sample, which does not show the plasticity in a normal compression condition. It was confirmed that plasticity newly appeared in the sample with Teflon tape (not shown here). Though we confirmed in the present study that even its relaxed sample showed appearance of plasticity (see Fig. 1), further research is required to investigate whether more brittle samples can show the same phenomenon for illustrating the broader effectiveness of the strategy.

One of the important conclusions from the framework what Sohn et al. suggested [34] and our current findings is that metallic glasses can be used in many engineering applications as long as strain/stress gradients are presented. Such gradients can be a consequence of the geometry of the sample and the presented strain/stress field. If we could

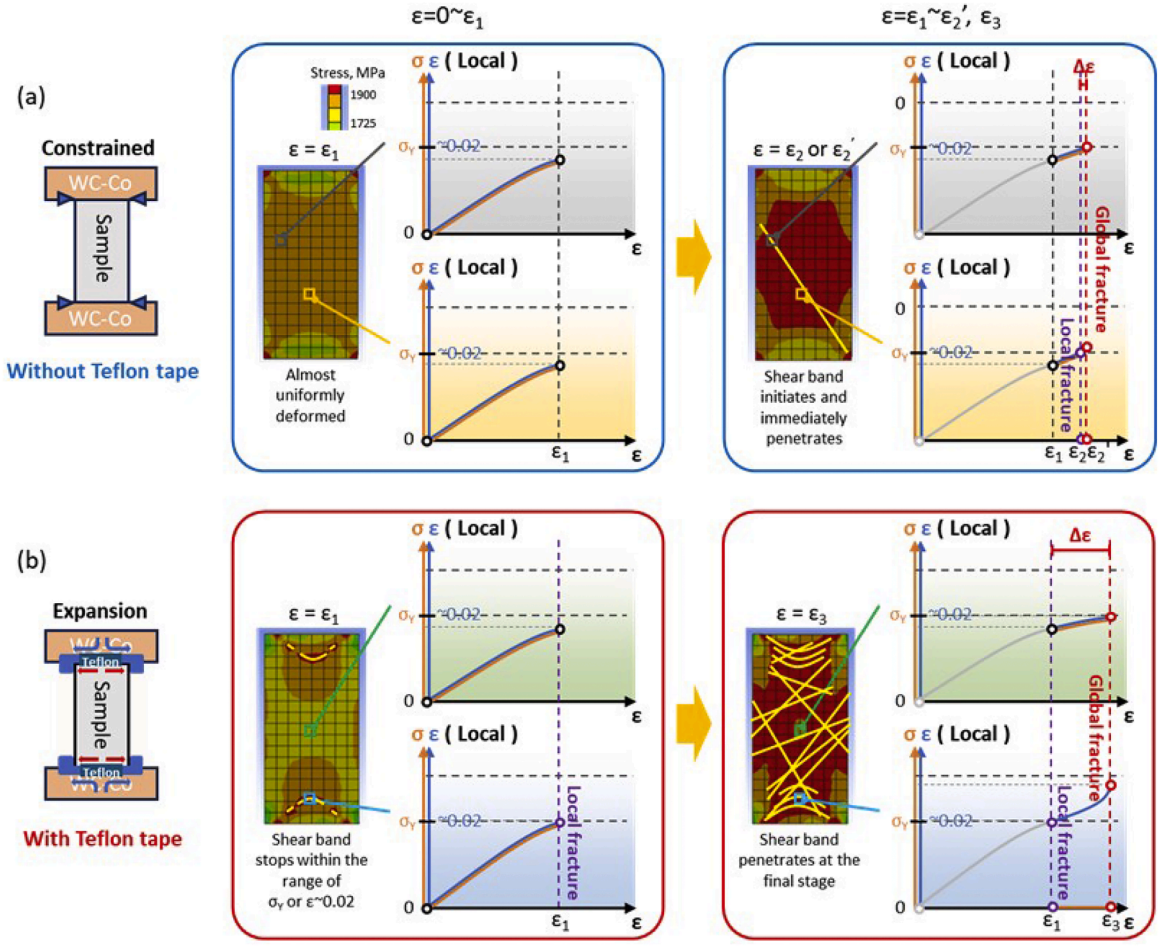

Fig. 5. Predicted fracture behaviour of the sample for (a) Case 1 (no Teflon tape used) and (b) Case 2 (Teflon tape inserted). The horizontal axis shows the global strain. Here, the local stress is assumed to be zero when the shear band penetrates. For Case 1, the local stress/strains were almost uniform, resulting in a short strain interval ($\Delta\varepsilon=\varepsilon_2'-\varepsilon_2$) between the first appearance of local fracture and global fracture. For Case 2, the expansion condition resulted in an inhomogeneous local strain/stress distribution, which induced gradual local fracture throughout the sample. The resulting strain interval ($\Delta\varepsilon=\varepsilon_3-\varepsilon_1$) was sufficiently long to prevent the occurrence of abrupt fracture in the sample.

design products while accurately understanding the states, it is expected that engineering applications of metallic glasses can be largely widened. Furthermore, if we can strategically tailor such presented strain/stress fields [e.g. by intentionally introducing gradient of mechanical properties (Young's modulus etc.) within the sample with the aim of creating a non-uniform local strain/stress distribution under applied stress], it is expected that not only compression but also other mechanical modes (e.g. tension or bending) to exhibit the improvement/appearance of plasticity. It will lead to the development of mechanically reliable and sustainable metallic glasses in the future.

In this study, the origin of plasticity in a relaxed $Zr_{50}Cu_{40}Al_{10}$ sample with inserted Teflon tape was identified by comparison against the sample behaviour under normal compression. Both experimental DIC and FEM analyses showed that the contact area between the loading platen and sample was constrained under normal compression and expanded laterally upon Teflon tape insertion. The expansion condition induced a complex inhomogeneous strain/stress distribution throughout the sample. Compared with normal compression, a shear band/crack initiated at a lower strain but penetrated the rest of the sample at a later stage of compression, during which multiple shear bands/cracks appeared. The expansion condition prevented immediate yielding and delayed final fracture in the sample, resulting in the emergence of plasticity.

CRediT authorship contribution statement

Rui Yamada: Writing – original draft, Resources, Investigation, Funding acquisition, Formal analysis, Conceptualization. **Keisuke Tabaru:** Investigation, Formal analysis. **Ryota Maeda:** Investigation, Formal analysis. **Wook Ha Ryu:** Methodology, Conceptualization. **Junji Saida:** Writing – review & editing, Supervision, Resources, Project administration, Funding acquisition, Conceptualization.

Declaration of competing interest

The authors declare that they have no known competing financial interests or personal relationships that could have appeared to influence the work reported in this paper.

Acknowledgements

We acknowledge Joe Yoshikawa from the Industrial Technology Institute, Miyagi Prefectural Government (ITIM) for assistance with the FEM simulations. We thank Edanz (https://jp.edanz.com/ac) for editing a draft of this manuscript.

This work was supported by a Grant-in-Aid from the Ministry of Education, Sports, Culture, Science and Technology, Japan, Scientific Research (A) (grant numbers 18H03829 and 23H00228); the Promoted Program for Interdisciplinary Research of the Frontier Research Institute

for Interdisciplinary Sciences (FRIS), Tohoku University; and a JSPS KAKENHI Grant-in-Aid for Scientific Research (C) (grant number 21K04899).

References

[1] A. Inoue, B.L. Shen, C.T. Chang, Super-high strength of over 4000 MPa for Fe-based bulk glassy alloys in $[(Fe_{1-x}Co_x)_{0.75}B_{0.2}Si_{0.05}]_{96}Nb_4$ system, Acta Mater. 52 (2004) 4093–4099.

[2] M.F. Ashby, A.L. Greer, Metallic glasses as structural materials, Scr. Mater. 54 (2006) 32–326.

[3] J. Schroers, Processing of bulk metallic glass, Adv. Mater. 22 (2010) 1566–1597.

[4] K. Gao, X.G. Zhu, L. Chen, W.H. Li, X. Xu, B.T. Pan, W.R. Li, W.H. Zhou, L. Li, W. Huang, Y. Li, Recent development in the application of bulk metallic glasses, J. Mater. Sci. Technol. 131 (2022) 115–121.

[5] B. Sarac, J. Eckert, Thermoplasticity of metallic glasses: Processing and applications, Prog. Mater. Sci. 127 (2022) 100941.

[6] S. Sohrabi, J. Fu, L. Li, Y. Zhang, X. Li, F. Sun, J. Ma, W.H. Wang, Manufacturing of metallic glass components: Processes, structures and properties, Prog. Mater. Sci. 144 (2024) 101283.

[7] D. Hofmann, J.Y. Suh, A. Wiest, G. Duan, M.L. Lind, M.D. Demetriou, W. L. Johnson, Designing metallic glass matrix composites with high toughness and tensile ductility, Nature 451 (2008) 1085–1089.

[8] D. Hofmann, Shape memory bulk metallic glass composite, Science 329 (2010) 1294–1295.

[9] D.V. Louzguine-Luzgin, Y. Zeng, A.D.H. Setyawan, N. Nishiyama, H. Kato, J. Saida, A. Inoue, Deformation behavior of Zr- and Ni-based bulk glassy alloys, J. Mater. Res. 22 (2007) 1087–1092.

[10] J. Saida, A.D. Setyawan, H. Kato, M. Matsushita, A. Inoue, Tailoring thermally induced nano-quasicrystallization and deformation-assisted nanocrystallization for mechanical property improvement in Zr-Al-Ni-Cu-Pd bulk metallic glasses, Mater. Trans. 50 (2009) 2079–2086.

[11] W. Guo, H. Kato, R. Yamada, J. Saida, Fabrication and mechanical properties of bulk metallic glass matrix composites by in-situ dealloying method, J. Alloys Compd. 707 (2017) 332–336.

[12] L.Y. Chen, A.D. Setyawan, H. Kato, A. Inoue, G.Q. Zhang, J. Saida, X.D. Wang, Q. P. Cao, J.Z. Jiang, Free-volume-induced enhancement of plasticity in a monolithic bulk metallic glass at room temperature, Scr. Mater. 59 (2008) 75. -58.

[13] J. Pan, Y.P. Ivanov, W.H. Zhou, Y. Li, A.L. Greer, Strain-hardening and suppression of shear-banding in rejuvenated bulk metallic glass, Nature 578 (2020) 559–562.

[14] W. Guo, R. Yamada, J. Saida, Rejuvenation and plasticization of metallic glass by deep cryogenic cycling treatment, Intermetallics 93 (2018) 141–147.

[15] W. Guo, T. Niiyama, R. Yamada, M. Wakeda, J. Saida, Synthesis and mechanical properties of highly structure-controlled Zr-based metallic glass by thermal rejuvenation technique, J. Phys.: Condensed Matter 35 (2023) 154004.

[16] S. Scudino, B. Jerliu, S. Pauly, K.B. Surreddi, U. Kuhn, J. Eckert, Ductile bulk metallic glasses produced through designed heterogeneities, Scr. Mater. 65 (2011) 815–818.

[17] Y. Zhang, W.H. Wang, A.L. Greer, Making metallic glasses plastic by control of residual stress, Nat. Mater. 5 (2006) 857–860.

[18] W.H. Ryu, R. Yamada, J. Saida, Tailored hardening of ZrCuAl bulk metallic glass induced by 2D gradient rejuvenation, NPG Asia Mater 12 (2020) 52.

[19] Y. Tang, H. Zhou, H. Lu, X. Wang, Q. Cao, D. Zhang, W. Yang, J.Z. Jiang, Extra plasticity governed by shear band deflection in gradient metallic glasses, Nat. Commun. 13 (2022) 2120.

[20] R. Yamada, W.H. Ryu, H. Isano, T. Yoshikawa, J. Saida, Creation of a 3D glassy state by thermal gradient treatment in a monolithic metallic glass, Adv. Eng. Mater. 26 (2024) 2401517.

[21] Y. Zhang, W.H. Wang, A.L. Greer, Making metallic glasses plastic by control of residual stress, Nat. Mater. 5 (2006) 857–860.

[22] Q. Wang, Y. Yang, H. Jiang, C.T. Liu, H.H. Ruan, J. Lu, Superior tensile ductility in bulk metallic glass with gradient amorphous structure, Sci. Rep. 4 (2014) 4757.

[23] L. Zhao, D. Han, S. Guan, X. Lu, K. Chan, G. Wang, Simultaneous improvement of plasticity and strength of metallic glasses by tailoring residual stress: Role of stress gradient on shear banding, Mater. Des. 197 (2021) 109246.

[24] R.M.O. Mota, E.T. Lund, S. Sohn, D.J. Browne, D.C. Hofmann, S. Curtarolo, A.F. D. Walle, J. Schroers, Enhancing ductility in bulk metallic glasses by straining during cooling, Commun. Mater. 2 (2021) 23.

[25] W.F. Wu, C.Y. Zhang, Y.W. Zhang, K.Y. Zeng, Y. Li, Stress gradient enhanced plasticity in a monolithic bulk metallic glass, Intermetallics 16 (2008) 1190–1198.

[26] S. Scudino, K.B. Surreddi, G. Wang, J. Eckert, Enhanced plastic deformation of $Zr_{41.2}Ti_{13.8}Cu_{12.5}Ni_{10}Be_{22.5}$ bulk metallic glass by the optimization of frictional boundary restraints, Scr. Mater. 62 (2010) 750–753.

[27] J. Hu, B.A. Sun, Y. Yang, C.T. Liu, S. Pauly, Y.X. Weng, J. Eckert, Intrinsic versus extrinsic effects on serrated flow of bulk metallic glasses, Intermetallics 66 (2015) 31–39.

[28] S. Scudino, K.B. Surreddi, G. Wang, G. Liu, Effect of stress concentration on plastic deformation of $Zr_{41.2}Ti_{13.8}Cu_{12.5}Ni_{10}Be_{22.5}$ bulk metallic glass under compressive loading, Mater. Lett. 179 (2016) 202–205.

[29] W.H. Ryu, W.S. Ko, H. Isano, R. Yamada, H. Ahn, G.H. Yoo, K.N. Yoon, E.S. Park, J. Saida, Sustainable steady-state serrated flow induced by modulation deformation sequence in bulk metallic glass, J. Alloys Compd. 946 (2023) 169308.

[30] H. Suzuki, R. Yamada, S. Tsubaki, M. Imafuku, S. Sato, T. Watanuki, A. Machida, J. Saida, Investigation of elastic deformation mechanism in as-cast and annealed eutectic and hypoeutectic Zr-Cu-Al metallic glasses by multiscale strain analysis, Metals 6 (2016) 12.

[31] O. Glushko, R. Pippan, D. Sopu, C. Mitterer, J. Eckert, How to catch a shear band and explain plasticity of metallic glasses with continuum mechanics, Nat. Commun. 15 (2024) 5601.

[32] D. Sopu, F. Moitzi, N. Mousseau, J. Eckert, An atomistic-level perspective of shear band formation and interaction in monolithic metallic glasses, Appl. Mater. Today 21 (2020) 100828.

[33] X. Yuan, D. Sopu, J. Eckert, Origin of strain hardening in monolithic metallic glasses, Phys. Rev. B 103 (2021) L140107.

[34] S. Sohn, N. Liu, G.H. Yoo, A. Ochiai, J. Chen, C. Levitt, G. Liu, S.C. Schroers, E. T. Lund, E.S. Park, J. Schroers, A framework for plasticity in metallic glasses, Materialia 31 (2023) 101876.